A simulation-based framework for earthquake risk-informed and people-centred decision making on future urban planning

Gemma Cremen [1], Carmine Galasso[1,2], John McCloskey[3]

[1]University College London, Department of Civil, Environmental and Geomatic Engineering, London, WC1E 6BT, United Kingdom
[2]Scuola Universitaria Superiore (IUSS) Pavia, Pavia, 27100, Italy
[3]University of Edinburgh, School of GeoSciences, Drummond St, Edinburgh, EH8 9XP, United Kingdom

1 Abstract

Numerous approaches to earthquake risk modelling and quantification have already been proposed in the literature and/or are well established in practice. However, most of these procedures are designed to focus on risk in the context of current static exposure and vulnerability, and are therefore limited in their ability to support decisions related to the future, as yet partially unbuilt, urban landscape. We propose an end-to-end risk modelling framework that explicitly addresses this specific challenge. The framework is designed to consider the earthquake (ground-shaking) risks of tomorrow's urban environment, using a simulation-based approach to rigorously capture the uncertainties inherent in future projections of exposure as well as physical and social vulnerability. The framework also advances the state-of-practice in future disaster risk modelling by additionally: (1) providing a harmonised methodology for integrating physical and social impacts of disasters that facilitates flexible characterisation of risk metrics beyond physical damage/asset losses; and (2) incorporating a participatory, people-centred approach to risk-informed decision making. The framework is showcased using the physical and social environment of an expanding synthetic city. This example application demonstrates how the framework may be used to make policy decisions related to future urban areas, based on multiple, uncertain risk drivers.

2 Introduction

Many earthquake risk-modelling approaches and computational tools for quantifying the consequences of seismic events on urban environments (e.g., direct and indirect physical damage, economic and social losses) already exist in the literature. For example, one of the most well-established natural-hazard (including earthquake) risk computational platforms is HAZUS (Hazards United States) (FEMA, 2018), which is used to calculate city-wide seismic losses across at least four continents (Freddi et al., 2021). Other procedures include MAEviz (Mid-America Earthquake Center Seismic Loss Assessment System) (Elnashai et al., 2008), SELENA (Seismic Loss Estimation using a Logic Tree Approach) (Molina et al., 2010), the OpenQuake Engine (Silva et al., 2014), and CAPRA (Comprehensive Approach to Probabilistic Risk Assessment) (Daniell et al., 2014) . Recent state-of-the-art achievements like the FEMA P-58 methodology (FEMA, 2018) facilitate earthquake risk quantification at a finer resolution, offering the ability to conduct detailed structure-specific loss assessments that enable more informed decision-making for individual assets (Cremen, Seville, & Baker, 2020).

These tools have mainly been used to quantify earthquake risk in the context of the present day, and are designed for static (and often deterministic) representations of exposure and seismic vulnerability. This significantly inhibits their ability to be implemented in future earthquake risk-mitigation planning. Given that climate change (e.g., M. G. Stewart & Deng, 2015; Yang & Frangopol, 2020), rapid population growth (e.g., Yang & Frangopol, 2019; Muis et al., 2015) and urbanisation are expected to significantly

change the urban landscape (in terms of both exposure and seismic vulnerability) in the coming decades, this is a generationally important issue. For example, UN-Habitat forecast that by 2050 some 70% of the world population will live in cites, adding some two billion citizens to the cities of the developing world (Habitat, 2020). Reducing disaster risk in new developments built to accommodate these new citizens is urgent and essential. While some attempts have been made in the literature to model earthquake risk (or some of its components) from a future-focused perspective (e.g., Calderón & Silva, 2021; Lallemant et al., 2017; Motamed et al., 2020; Wyss, 2005; Lallemant, 2015), there remain a number of limitations associated with the state-of-the art in this space.

Firstly, future earthquake risk studies have predominantly focused on the evolution of exposure and vulnerability in the context of the (physical) built environment, failing to consider the effect of sociodemographic changes that are an important part of community resilience planning (Sutley et al., 2017). This means that they quantify earthquake risk in terms of traditional metrics like physical asset losses and casualties, which are narrow dimensions of impact (Walsh & Hallegatte, 2020) that do not account for the disproportionate consequences of disasters on vulnerable, low-income groups, for instance (e.g., Markhvida et al., 2020; Verschuur et al., 2020; Adnan et al., 2020). These studies are consequently missing a people-centred (ideally participatory) approach to future earthquake risk assessment (e.g., Scolobig et al., 2015; I. S. Stewart et al., 2017), which is actively encouraged by forward-looking international agreements on disaster risk management like the 2015-2030 Sendai Framework for Disaster Risk Reduction (Aitsi-Selmi et al., 2016). Shortcomings of existing future earthquake risk assessment approaches stem from the general lack of a commonly agreed framework for modelling tomorrow's risks from natural hazards.

This study attempts to overcome these limitations, by proposing a comprehensive end-to-end simulation-based framework for quantifying future earthquake ground-shaking risk. The proposed framework can be used as part of an effective support environment for urban development decision making. Here we use the word 'environment' to indicate the potential for iterative engagement with stakeholders to evolve optimised low-risk solutions within externally imposed constraints. Hence, the proposed framework is more than just a risk model or computational tool but provides an environment to support risk-sensitive planning decisions, incorporating a participatory approach to risk understanding and quantification that can account for diverse stakeholder priorities towards different dimensions of risk (see Galasso et al., 2021). The stakeholder steps into the process and is encouraged to engage with its functionality, potentially modifying its construction and many of its assumptions. It is an invitation to co-production, providing decision support rather than a tool to usurp authority. In addition, it includes a harmonious integration of physical and social impact quantification that (1) explicitly accounts for uncertainties in the future projections of underlying variables (e.g., asset location and structural or nonstructural features, building fragility, age and income profile of inhabitants); and (2) facilitates a flexible approach to risk measurement beyond conventional asset losses. We apply the framework to the hypothetical city of "Futureville", showcasing its ability to support decisions related to policy-making for the communities of tomorrow.

This paper is structured as follows. The framework is introduced and described in Section 3. Section 4 applies the framework to the city of "Futureville", demonstrating how it can be used to determine the optimum future-focused policy according to different sets of stakeholder risk priorities. Section 5 highlights the versatility of the proposed framework, showcasing its ability to adapt to alternative assumptions and/or additional uncertainties in the underlying risk calculations. Conclusions of the paper are finally provided in Section 6.

3 Proposed Framework

The proposed framework for earthquake risk-informed, people-centered future urban development is presented in Figure 1, and is composed of four main calculation stages (or modules): (1) Seismic Hazard Module; (2) Engineering Impact Module; (3) Social Impact Module; and (4) Decision Module. For a specific temporal instant in the future, each ith iteration of the framework evaluates the risk associated with a set of "hard" (i.e., directly related to the physics of the built environment, such as urban design that could constrain the location of future development and building code improvement) and/or "soft" (e.g., social safety nets, post-disaster financing or insurance) policies to be implemented, with the ultimate aim of identifying the policy option leading to the minimum risk outcome. In this context, risk refers to the collective values of collaboratively selected risk metrics that are weighted in line with the priorities of stakeholders (e.g., administrative authorities responsible for future urban development and related policy implementation and/or relevant community representatives). Monte Carlo simulation is used to capture uncertainties in the calculations, such that random variables included as part of Modules (1) to (3) are sampled N_s times at the specific temporal instant of interest, to produce the risk-metric values that act as input to Module (4) in each iteration. During the first iteration, the framework provides flexibility to modify the considered risk metrics through a participatory process, which may require additional data collection and calculations in Modules (2) and (3). The components of the framework are now briefly explained, and are described in more detail for a case-study demonstration in Section 4.

1. **Seismic Hazard Module:** This module contains calculations related to the earthquake ground-shaking hazard of interest. This hazard could be expressed in the form of a scenario earthquake, with a prescribed rupture (i.e., magnitude, location, etc.) that produces either deterministic or uncertain ground-motion fields across target locations. The hazard could also be represented probabilistically, accounting for uncertainty in the rupture features within a specified time frame (e.g., Iacoletti et al., 2021). However, time-based seismic hazard assessments are more likely to appeal to the insurance sector rather than public policy makers (Bonstrom et al., 2012). The scenario approach (as opposed to probabilistic seismic hazard analysis) is particularly beneficial for communicating risk to a policy maker or to communities, who may not have an intuitive sense of probability and the dynamic discounting of financial assets (Bonstrom et al., 2012). Since ground-motion variability can dominate the uncertainty associated with scenario-based seismic risk calculations (e.g., Markhvida et al., 2020), adopting a fully deterministic earthquake scenario is useful for obtaining a more comprehensive understanding of risk changes that are specifically related to the different policies of interest. The outputs of this module are ground-motion field estimates across a number of locations of interest (i.e., close to where assets/infrastructure at risk are located).
These fields can be sampled from a ground-motion model (GMM), for instance, which describe probability density functions of different ground-motion intensity measures (i.e., descriptions of the strength of shaking) that are conditional on properties of the earthquake source, wave path, and site-specific characteristics (e.g., Stafford et al., 2008). GMMs typically have the following functional form (e.g., Cremen, Werner, & Baptie, 2020):

$$\log(im_{obs,n_e,n_r}) = \log(im_{GMM,n_e,n_r}) + z_{E,n_e}\sigma_E + z_{A,n_e,n_r}\sigma_A \quad (1)$$

where, for the n_eth event, $\log(im_{obs,i,j})$ is the logarithm of the predicted intensity measure for the ground-motion field at the n_rth point; $\log(im_{GMM,n_e,n_r})$ is the corresponding logarithm of the GMM's median estimated intensity measure given certain variables (related to source, path, and site effects) and model parameters; z_{E,n_e} is the normalised inter-event residual (common across the ground-motion field of the n_eth event); and z_{A,n_e,n_r} is the normalised intra-event residual (that captures site-to-site variations in the ground-motion field). σ_E and σ_A are the GMM's

inter-event and intra-event standard deviations, respectively. Models that account for correlations between the intra-event residuals at different locations - due to similarities in experienced wave path and fault distance - are often used in conjunction with GMMs, for more accurate representations of ground-motion fields and resulting damage/losses (e.g., Weatherill et al., 2015).
Alternatively, ground-motion fields can be numerically simulated using physics-based models of source, path, and site effects (e.g., Graves et al., 2011) that are capable of computing the complete ground-motion time series. Physics-based simulations can lead to ground-motion predictions of similar or higher quality than statistically-driven GMMs (with lower uncertainty) (e.g., Bradley, 2019), but require significantly longer computational time and extensive input data that can prohibit their widespread use (e.g., Freddi et al., 2021).

2. **Engineering Impact Module:** This module conducts calculations for assessing earthquake-induced physical damage (structural and nonstructural) to the future built environment (including buildings and critical infrastructure). The outputs of this module are damage and/or direct asset loss estimates (e.g., repair cost, casualties, asset downtime).
Damage can be computed using building-level fragility functions for instance, which translate measures of ground-motion intensity (recorded or simulated at or near a given asset of interest) into probabilities of collapse and/or other limit (or damage) states of interest (Porter et al., 2007). Losses may then be computed using damage-to-loss models that relate different damage states to various degrees of consequences, or vulnerability functions that estimate losses directly from ground-motion intensity measures (Martins & Silva, 2020). Fragility functions, damage-to-loss models, and vulnerability functions can be obtained analytically, using the results of structural analyses that incorporate physics-based representations of the built environment (e.g., Pitilakis et al., 2014; Silva et al., 2019; Baker, 2015). They may also be empirically derived, based on damage data collected during past earthquakes (e.g., Maqsood et al., 2016; Gautam et al., 2018). Interconnected infrastructure losses (e.g., downtime of a water or gas pipelines or road network) can be estimated using network analysis techniques that aggregate asset-specific consequences and account for inter-asset functionalities (e.g., Esposito et al., 2015; Guidotti et al., 2016).
The exact spatial and physical configuration of the built environment (denoted as "conditional urban plan" in Figure 1) can depend on projections of future population and land-use (Seto et al., 2012), as well as the potentially time-dependent vulnerability of engineering assets (Mondoro et al., 2018; Lallemant et al., 2017). Any proposed hard policies (such as structural or nonstructural improvements, building-code upgrades, and critical infrastructure relocation) will also influence the details of the future built environment.

3. **Social Impact Module:** This module is used to enrich the asset loss estimates of the Engineering Impact Module on the basis of socio-economic and/or demographic projections. For example, Engineering Impact Module calculations of damage to commercial buildings could be combined in the Social Impact Module with data on the industrial flow of goods, to determine earthquake-induced impacts on the productivity of different economic sectors (Markhvida et al., 2020). This module also facilitates the disaggregation of asset losses in terms of socio-economic/demographic factors such as income level, age, or gender, which could be derived from census data or household surveys (among other sources). For instance, road network downtime outputs of the Engineering Impact Module can be attributed spatially to different socio-economic groupings, to determine accessibility losses across specific wealth classes (Miller & Baker, 2016).
The introduction of soft policies (related to disaster insurance or enhanced post-event liquidity access, for instance) can influence the coping capacity or response of different social systems to the hazard of interest, and therefore can alter the data

examined in this module. The outputs of this module are used to construct risk metrics for decision making.

4. **Decision Module:** This module leverages stakeholder feedback in a participatory process to determine: (1) the n_{final} ultimate risk metrics to be considered based on outputs of the Social Impact Module. This step is necessary for the first framework iteration only, when $n_{initial}$ metrics initially proposed by the modeller are modified and finalised according to stakeholder perspectives; and (2) the weights to be placed on each finalised risk metric, in line with decision-maker risk priorities. Values for (2) can be obtained according to the analytic hierarchy process (Saaty, 1980), for instance. This procedure involves the stakeholders comparing the relative importance of pairs of risk metrics on a scale from 1/9 to 9, where 1 indicates both metrics are equally significant, 5 implies that risk metric #1 is strongly important over risk metric #2, 9 indicates that risk metric #1 is significantly more important than risk metric #2, and reciprocal values imply inverse opinions. Weights w_j for each metric are equivalent to the principal right eigenvector of a $n_{final} \times n_{final}$ matrix that summarises the quantitative results of the comparison.
5. **Policy with Lowest Overall Risk:** This calculation uses the outputs of the Decision Module across all n_{policy} examined policies in a decision-making algorithm to determine the overall risk associated with each policy. TOPSIS (Technique for Order of Preference by Similarity to Ideal Solution; Yoon & Hwang, 1995) is one such decision-making approach that could be used in this module. This multi-criteria decision-making methodology first involves normalising the risk-metric values according to:

$$r_{ij} = \frac{x_{ij}}{\sqrt{\sum_{k=1}^{n_{policy}} x_{kj}^2}} \tag{2}$$

where x_{ij} is the magnitude of the jth risk metric for the ith policy. Then, the total distance of a given policy from the best and worst policies are respectively computed as:

$$y_i^+ = \sqrt{\sum_{j=1}^{2} (v_j^+ - r_{ij} w_j)^2} \tag{3}$$

and

$$y_i^- = \sqrt{\sum_{j=1}^{2} (v_j^- - r_{ij} w_j)^2} \tag{4}$$

Both r_{ij} and w_j are as previously defined. v_j^+ and v_j^- respectively denote the most ideal (i.e., minimum) and most non-ideal (i.e., maximum) values of $r_{ij} w_j$ across all examined policies. Finally, the best policy is deemed to be that with the largest S_i value, calculated from:

$$S_i = \frac{y_i^-}{y_i^- + y_i^+} \tag{5}$$

4 Case-Study Description

The virtual urban area examined here is a heavily altered version of the Centerville Virtual Community introduced in Ellingwood et al. (2016) (Figure 2), herein referred to as "Futureville". Futureville exists on the same 104 km^2 physical footprint as Centerville, but excludes for simplicity prominent geographical features (i.e., the hills and water bodies, given the focus on earthquake hazard only) and contains a modified set of Centerville's engineered assets (see Section 4.2). Futureville is divided into 9 building zones, four of which (i.e., Zones 6 to 9) are yet to be developed. We specifically assess the implementation of policies at 2050, which is the target year for which Zones 6

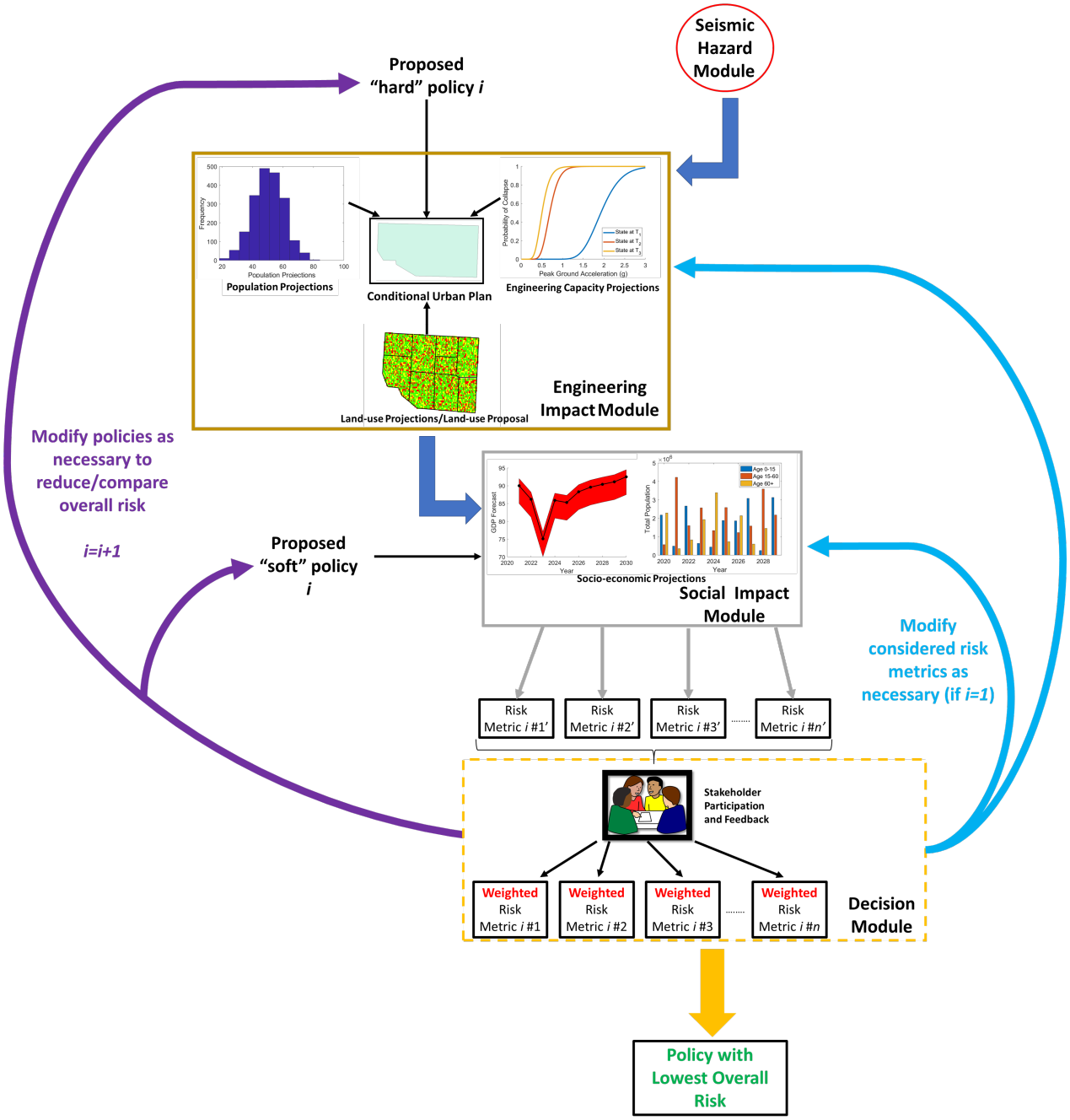

Figure 1: Proposed simulation-based framework for earthquake risk-informed and people-centred future planning.

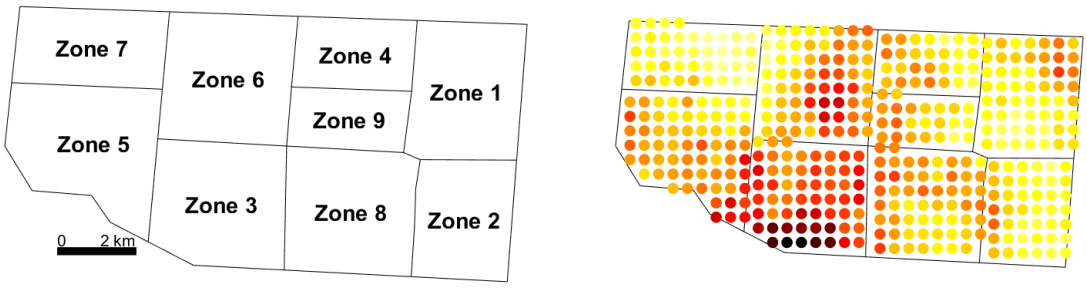

Figure 2: (a) Physical outline of the "Futureville" case study urban area and (b) the set of PGA values associated with the selected (fully deterministic) scenario earthquake (see Section 4.1).

to 9 are intended to be built. 1,000 Monte Carlo simulations are used for each policy iteration, which was found to produce reasonably stable results for the various framework outputs.

4.1 Seismic Hazard Module

We adopt a fully deterministic scenario-based approach for this study, assuming that the event of interest is a magnitude 7 earthquake that occurs on a vertical strike-slip fault situated approximately 30 km southwest of Futureville. The only ground-motion intensity measure examined in this case is peak ground acceleration (PGA), given the format of the fragility functions used as part of the Engineering Impact Module (see Section 4.2). We first use the Boore et al. (2014) GMM to sample 1,000 sets of PGA values on a 500 m $\times$ 500 m grid within each polygon of Futureville (assuming a uniform $Vs30$ value of 500 m/s across the city), incorporating spatial correlation in the intraevent term of the GMM using the model of Jayaram and Baker (2009). We then base the selected scenario on the set that produces the 75th percentile mean PGA value across all locations; this set is used for all N_s Monte Carlo simulations of the analysis. Figure 2(b) displays the chosen set of ground motions.

4.2 Engineering Impact Module

The Engineering Impact Module focuses exclusively on buildings for this case study. Zones 1 to 3 of "Futureville" are current residential zones, composed of only low-rise dwellings (i.e., light-frame wood buildings classified as W1 in FEMA, 2018), and contain a total of 8,309 buildings to serve the current (2021) Futureville population of 27,250 (note that the buildings in each zone are randomly positioned across a 20m spaced grid). These zones are respectively associated with the same proportional distribution of building codes as the original Centerville Virtual Community z1 (52% of buildings are not seismically designed, 47% have low strength and ductility, 1% have moderate strength and ductility), z2 (69% are not seismically designed and 31% have low strength and ductility) and z5 (100% are not seismically designed). Each current residential zone also contains one school (with the same characteristics as the RC3 structural type in the original Centerville, i.e., low-rise concrete moment frame with moderate strength and ductility) and one grocery store (with the same characteristics as the S2 structural type - steel light frame with low strength and ductility - in the original Centerville) located at/near its centroid.

Zone 4 is a current retail/business zone containing 66 buildings randomly distributed across a 110m-spaced grid, with the same proportional distribution of structure types as z9 of the original Centerville (31% of buildings are low-rise steel braced frame with low strength and ductility, 14% are low-rise concrete moment frame with low strength and ductility, 49% are low-rise reinforced masonry bearing walls with wood or metal deck diaphragms that are not seismically designed, and 6% are steel light frame with low strength and ductility). Zone 5 is a current heavy and light industrial zone containing 134 buildings randomly distributed across a grid of 110m spacing, with 50% of these sharing the characteristics as buildings in z10 of the original Centerville (low-rise steel braced frame that is not seismically designed), and the other 50% sharing the same building characteristics as z11 of the original Centerville (low-rise steel braced frame with moderate strength and ductility). We assume that the current buildings of Centerville will still exist in 2050, and will have the same seismic capacity as now (i.e., the potential time-dependence of building seismic fragilities are neglected at this stage of the analysis).

Zones 6 to 8 will be future residential areas (with one grocery store and one school at/near their centroids) with the same type of building as Zones 1 to 3, and Zone 9 will be a future retail/business district with the same distribution of building types as Zone 4. All future buildings will be built to conform to the "high-code" description of FEMA (2018), i.e., they possess high strength and ductility. It is anticipated that the population of Futureville will grow broadly in line with a uniform distribution version of the Global United Nations Population Prospects for 2050 (United Nations, 2019). Thus, the total 2050 population for each kth Monte Carlo simulation is computed as follows:

$$p_{2050}^{k} = \frac{27,250}{\tilde{p}_{2020}} \sum_{age=1}^{n_{age}} F_{age}^{-1}(u_k) \tag{6}$$

where $F_{age}^{-1}(x)$ is an inverse uniform distribution between the lower and upper 80 percent prediction intervals of the 2050 global population projections provided in United Nations (2019) for a given age group (the results of which are reduced by 20% in the 18-25 years age category to accommodate out-of-town college students - see Section 4.3 - assuming an even age distribution of the population across the 15-19 year grouping), n_{age} is the total number of 5-year age groups considered in United Nations (2019), u_k is a random number between 0 and 1, $\tilde{p}_{2020}$ is the United Nations (2019) median projection of the world's total population in 2020, and 27,250 is the current population of Futureville. Since the exact layout of future development within Zones 6 to 9 is uncertain, the number and location of associated buildings varies for each simulation (see Figure 3). We assume that the number of residences is evenly distributed across Zones 6 to 8, and that for each Monte Carlo simulation, there are exactly enough buildings within these zones to facilitate the additional corresponding sampled Futureville population for 2050. We assume that the number of buildings within Zone 9 is equal to 5% of the total number of buildings in Zones 6 to 8. For each simulation, every building in Zones 6 to 8 is randomly assigned to one point on a 20m spaced grid, and each building in Zone 9 is randomly positioned on a 110m spaced grid.

Note that the damage state of each building within Futureville is randomly sampled for each Monte Carlo simulation according to the corresponding equivalent-PGA fragility functions in FEMA (2018) and using the PGA output of the Seismic Hazard Module closest to the building's location. A selection of these fragility functions are presented in Figure 4, to illustrate capacity differences between different structural types and building codes. Information presented in this section is summarised in Table 2.

4.3 Social Impact Module

This case study particularly focuses on socio-economic projections in terms of age and income (gender is not anticipated to be a defining vulnerability factor in 2050 Futureville). Zones 1 to 3 are respectively associated with the same median incomes as z1,

Table 1: Population projection data used in this study from United Nations (2019),), as well as the resulting expected population of Futureville in 2050 (indicated as "Expected"). Note that "Current" denotes the median population projection for 2020 (used in $\tilde{p}_{2020}$ of equation 6), "Lower" indicates the lower 80 percent projection for 2050 (used as part of $F_{age}^{-1}(x)$ in equation 6) and "Upper" indicates the upper 80 percent projection for 2050 (also used as part of $F_{age}^{-1}(x)$ in equation 6). Each column displays aggregated data across two five-year age groups, for brevity. Values are expressed in thousands.

Category	0-9	10-19	20-29	30-39	40-49	50-59	60-69	70-79	80-89	90-99	100+
Current	1,342,381	1,253,463	1,192,080	1,150,350	973,155	833,622	591,786	312,459	124,116	20,814	573
Lower	1,269,615	1,266,264	1,267,036	1,300,654	1,194,791	1,094,850	970,549	659,939	331,652	67,685	2,831
Upper	1,484,382	1,437,483	1,386,278	1,305,112	1,200,160	1,103,399	987,084	689,381	368,406	80,614	3,649
Expected	4,821	4,545	4,179	4,561	4,192	3,848	3,427	2,362	1,226	260	11

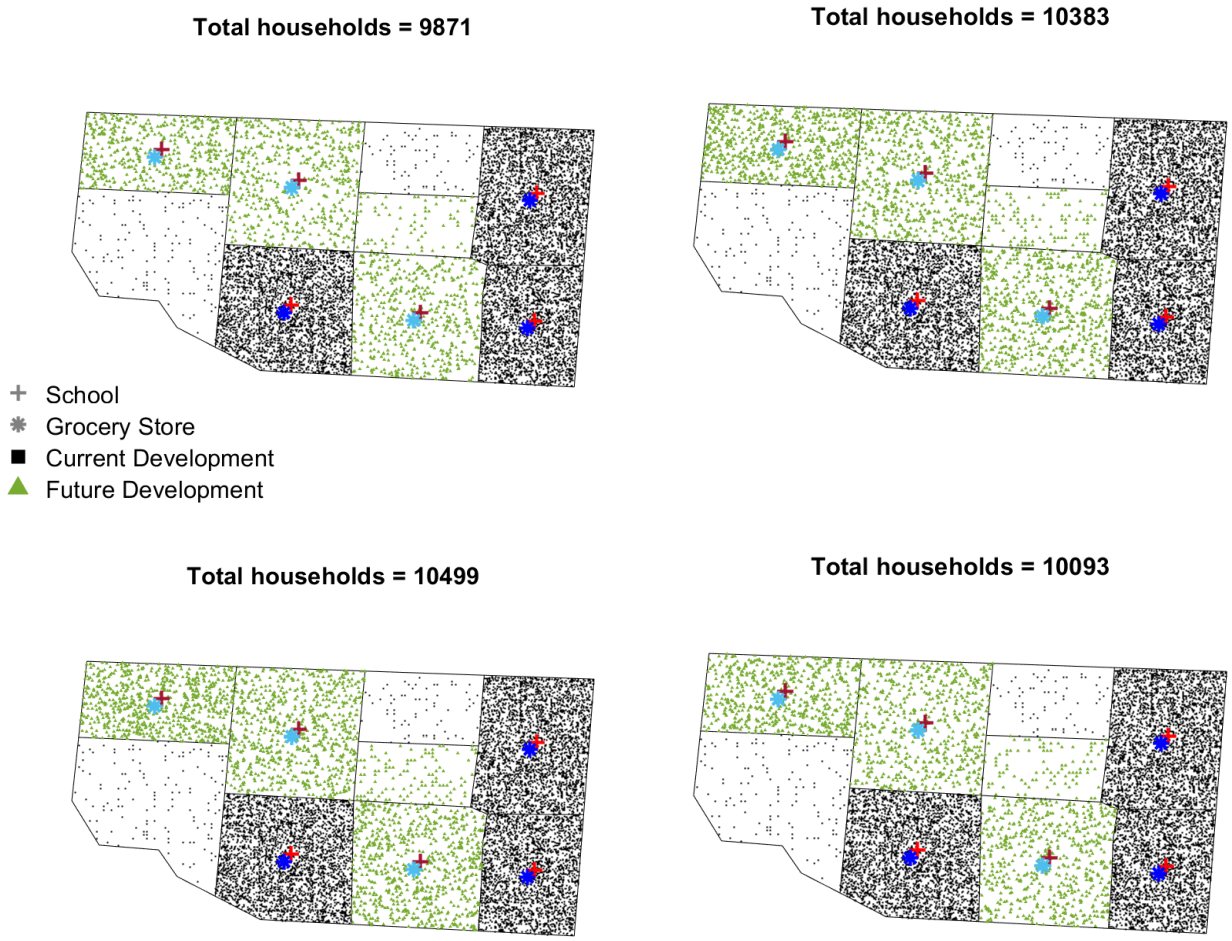

Figure 3: Current and future urban development in Futureville. Each subfigure displays a different Monte Carlo sample of future development in Zones 6 to 9 (see Figure 2). Note that each plotted point represents one building.

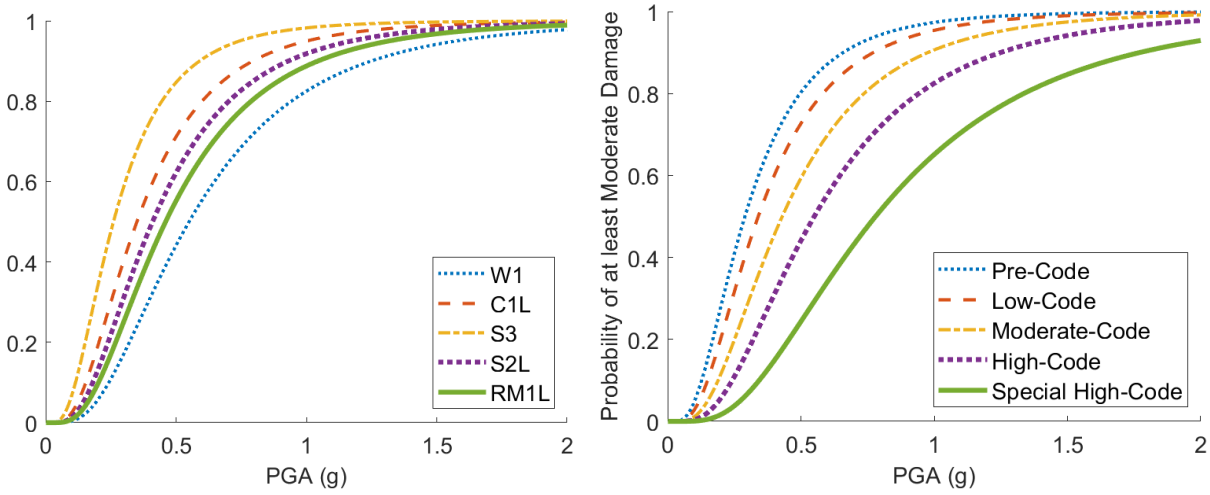

Figure 4: Various FEMA (2018) equivalent-PGA fragility functions that describe the probability of experiencing at least moderate damage, corresponding to (a) different structural types built to the "high-code" specification of FEMA (2018) and (b) light-frame wood buildings designed to different structural codes. W1 = light-frame wood, C1L = low-rise concrete moment frame, S3 = steel light frame, S2L = low-rise steel braced frame, and RM1L = low-rise reinforced masonry bearing walls with wood or metal deck diaphragms. Note that "pre-code", "low-code", "moderate-code", "high-code", and "special high-code" respectively correspond to the absence of seismic-resistant design, low strength and ductility, moderate strength and ductility, the "high-code" FEMA (2018) specification, and the case of maximum strength and ductility for a high seismic design level.

Table 2: A summary of Futureville zone information related to the Engineering Impact Module (see Section 4.2). Note that in the "Design-Code Distribution" column, "N" indicates an absence of seismic-resistant design, "L" implies low strength and ductility, "M" represents moderate strength and ductility, and "H" denotes the "high-code" FEMA (2018) specification.

Zone Number	Zone Type	Structural Type	Design-Code Distribution
1	Residential	Light-frame Wood (Housing)	52% N, 47% L, 1% M
		Low-rise Concrete Moment Frame (School)	100% M
		Light-frame Steel (Grocery Store)	100% L
2	Residential	Light-frame Wood (Housing)	69% N, 31% L
		Low-rise Concrete Moment Frame (School)	100% M
		Light-frame Steel (Grocery Store)	100% L
3	Residential	Light-frame Wood (Housing)	100% N
		Low-rise Concrete Moment Frame (School)	100% M
		Light-frame Steel (Grocery Store)	100% L
4	Retail/Business	Low-Rise Steel Braced Frame	100% L
		Low-Rise Concrete Moment Frame	100% L
		Low-Rise Reinforced Masonry Bearing Walls	100% N
		Light-frame Steel	100% L
5	Industrial	Low-rise Steel Braced Frame	100% N
		Low-rise Steel Braced Frame	100% M
6	Residential	Light-frame Wood (Housing)	100% H
		Low-rise Concrete Moment Frame (School)	100% H
		Light-frame Steel (Grocery Store)	100% H
7	Residential	Light-frame Wood (Housing)	100% H
		Low-rise Concrete Moment Frame (School)	100% H
		Light-frame Steel (Grocery Store)	100% H
8	Residential	Light-frame Wood (Housing)	100% H
		Low-rise Concrete Moment Frame (School)	100% H
		Light-frame Steel (Grocery Store)	100% H
9	Retail/Business	Low-Rise Steel Braced Frame	100% H
		Low-Rise Concrete Moment Frame	100% H
		Low-Rise Reinforced Masonry Bearing Walls	100% H

z2, and z5 in the original Centerville. Thus, Zone 1 may be broadly classed as "high income". Zone 2 may be described as "middle income", and Zone 3 can be categorised as "low income". Futureville's urban planners have provided the following details. Zone 6 will contain high-end residences that accommodate"high income" future residents, and the other two future residential zones will be populated with 50% middle- and 50% low-income housing. (Note that these future income/household distributions align with 2050 socioeconomic projections for the city, and income bands for current residential zones are not expected to vary in the future). Each household will depend on the nearest grocery store for food needs. It is anticipated (based on the city's most recent census) that all people under the age of 60 will live in a residential building with three other people, all others will live in a two-person building, and there will be no disabled members of Futureville's population. All children under the age of 18 will avail of the nearest school and will live with at least two older people. The exact inhabitant profile of each individual building in 2050 is currently uncertain, and is therefore randomly sampled in line with the age distribution of the simulated population (see equation 6) for each Monte Carlo simulation. While the proportion of college-going students among Futureville's population is currently negligible, a recent report commissioned by the city's administrators projects this to increase to 20% of all 18 to 25 year olds in 2050. Since Futureville does not (or will not) contain tertiary education facilities, we remove 20% of the simulated 18-25 year old population from our analysis.

It is understood that all people between the ages of 18 and 60 living in the city will work at some location within Futureville (but the exact workplace of each person is currently uncertain). Workplace buildings are randomly assigned to each worker in a household for a given Monte Carlo simulation, in accordance with the following information obtained from Futureville's most recent census (which is not expected to notably change by 2050). All high-income workers work in retail/business zones. Middle-income workers are distributed in the ratio 7:2:1 among retail/business, light industry, and heavy industry. Low-income workers are distributed in the ratio 4:3:3 among retail/business, light industry, and heavy industry. It is anticipated that retail workers of Zones 1 to 3 will work in Zone 4, whereas retail workers of Zones 6 to 8 will work in Zone 9. It is believed that all workers from the same household will work within the same Zone (but not necessarily the same building). A schematic summary of Futureville's engineering asset dependence across different demographic groups is presented in Figure 5.

4.4 Proposed Policies

We examine three hypothetical policies in this case (two hard and one soft), which are mutually exclusive (and therefore intended for individual implementation) due to budgetary constraints. Policy #1 involves retrofitting all buildings within the existing low-income Zone 3 to conform to FEMA (2018) high-code specification. Policy #2 provides financial support to facilitate a requirement that all buildings within future Zones 6 to 9 are instead built to "special high-code", and that all existing non-residential buildings with no seismic design are upgraded to FEMA (2018) high-code specification. Policy #3 provides post-disaster employment insurance to all workers and issues post-disaster repair assistance that covers minor damage to residential structures.

Note that Policy #1 and Policy #2 alter the types of fragility functions considered in the Engineering Impact Module for certain buildings. Both of these policies result in the replacement of fragility functions for retrofitted buildings with corresponding FEMA (2018) models that represent high strength and ductility. Special-code buildings stipulated in Policy #2 are modelled using appropriate equivalent-PGA special high-code fragility functions detailed in FEMA (2018) (see Figure 4 for further explanation and an example). It is assumed that Policy #3 eliminates the need for people to depend on their workplace for income, and therefore removes $W_{y,z}$ from the social network summarised in Fig-

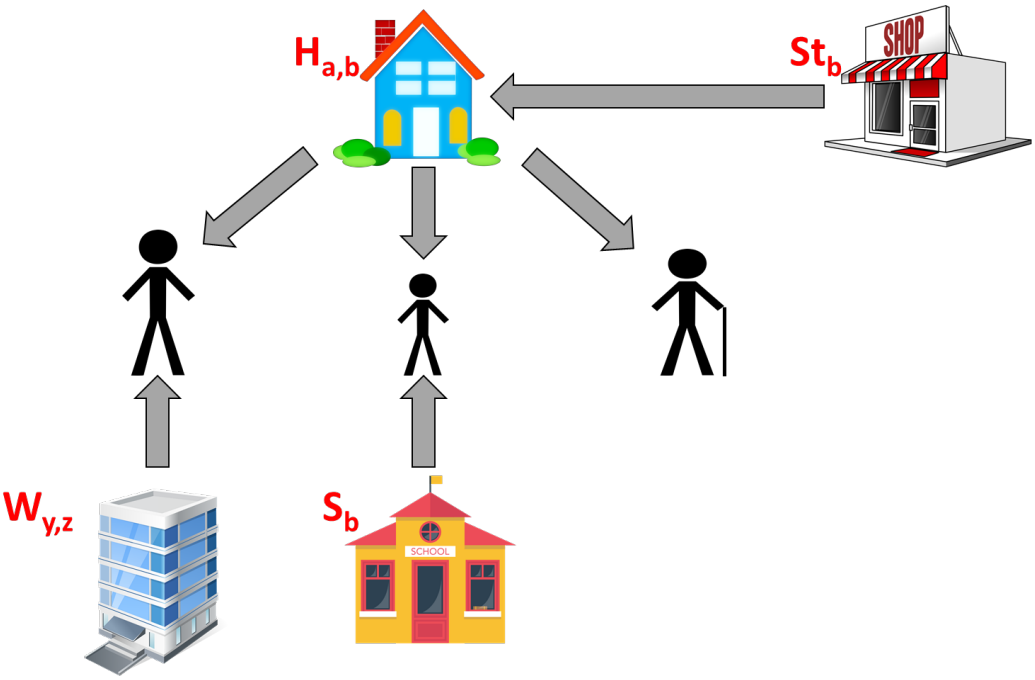

Figure 5: A graphical summary of asset dependence (i.e., the social network) for different demographic groups within Futureville. Within the bth zone, the ath household $H_{a,b}$ (containing either four people under the age of 60 or two people above this age) depends on the local grocery store St_b. Each adult inhabitant of $H_{a,b}$ under the age of 60 works at some workplace $W_{y,z}$ within a different (zth) zone. Each child inhabitant of $H_{a,b}$ attends the local school S_b.

ure 5. Policy #3 also avoids a self-funded payout in the case of minor residential damage, which may be particularly relevant for low-income households.

4.5 Initial Risk Metrics

We initially assume that $n_{initial} = 3$ risk metrics are of interest to stakeholders: (1) the expected proportion of the population that is displaced; (2) the expected proportion of the population that experiences some financial loss due to damage to their residence (i.e., at least minor damage for Policy #1 and 2, and at least moderate damage for Policy #3), and (3) the maximum expected proportion of casualties across any time of the day, all of which are disaggregated in terms of income band and age bracket. Note that the expected values for all risk metrics are obtained by averaging the corresponding quantities produced from the N_s Monte Carlo samples.

For assessing the initial risk metric (1), we assume that all occupants of a household will be displaced for a given Monte Carlo simulation if there is moderate damage to at least two nodes of their social network, which includes the residence itself, the nearest grocery store and can also (for relevant age groups) incorporate schools and workplaces (except in the case of Policy #3, as described in Section 4.4). The initial risk metric (3) is computed using the aggregate of all casualty rates (i.e., accounting for each casualty severity level, including minor injuries) provided in Tables 12-3 to 12-11 of FEMA (2018), according to each building type included in Futureville. It is assumed that all of Futureville's oldest (i.e., 60 or over) residents will be at home when the earthquake occurs, and those younger than 60 will be at their residence if the earthquake occurs at nighttime and/or on a weekend. For a weekday earthquake in the daytime or at commute time, it is assumed that all workers will be at work and that all children will be at school. The indoor/outdoor population distribution of a given building is obtained from Table 12-2 of FEMA (2018), using "Residential" occupancy values for casualties that occur at home, "Commercial" occupancy values for casualties in Zones 4 and 9, and "Industrial" occupancy values for casualties in Zone 5. We find that the maximum expected proportion of casualties occurs for a daytime earthquake on a weekday, which is therefore used as the temporal basis for initial risk metric (3).

Values of each initial risk metric are displayed in Figures 6 and 7 across the three examined policies; also shown for completeness are results for the case in which no policy is implemented, as well as median, 25th, and 75th percentile values to convey the underlying distributions. It is interesting to note that the expected proportion of the oldest age group displaced is significantly lower than that of younger age groups, for all cases. This may be explained by the fact that the displacement of the oldest age group does not depend on the functionality of either workplaces or schools. In the case of Policy #3 (where displacement of all ages is independent of workplace damage), the most affected age group is clearly young people, whose post-disaster displacement status (and that of the adults they live with) depends on the functionality of the nearest school (in addition to that of the grocery store and their place of residence).

The expected proportion of the population that experiences some financial loss due to residential damage is notably lower for Policy #3 than other cases, across all ages and income levels. This is because the level of damage that triggers self-funded repairs is higher for Policy #3 (i.e., moderate damage versus slight damage for other cases). A further noteworthy observation from Figure 7 is that while the proportion of the population experiencing loss due to residential damage for a given policy case is fairly constant across all age groups, there are some discrepancies in the value of this metric for different income groups, which vary for different policies. For example, the proportion of low-income households experiencing residential-damage-induced loss is significantly larger than that of higher income groups except for Policy #1 (as expected, since this policy particularly targets a low-income residential zone).

It can be seen that the total expected proportion of casualties is approximately 1% of the future projected population. The most affected age group in terms of casualties is adults under the age of 60, suggesting that the majority of casualties occur in workplaces. This conclusion is supported by the fact that Policy #2 - which involves retrofitting work buildings that have not been seismically engineered - significantly mitigates the discrepancy in casualties between age groups. The poorest residents of Futureville tend to suffer more casualties than those of other income groups, except in the case of the low-income targeted Policy #1.

There is noticeable uncertainty in the underlying distributions of initial risk metrics (1) and (3). This observation may be partially explained by the large dispersions that characterise FEMA (2018) equivalent-PGA fragility functions; the resulting uncertainties in damage states could be reduced using state-of-the-art structure-specific analytical fragility models that use more appropriate ground-motion intensity measures for damage quantification (e.g., Silva et al., 2019). The variability associated with initial risk metric (1) may also be caused by the dependence of this metric on the uncertain states of multiple engineered assets. The breadth of the distribution underlying initial risk metric (3) can be partially attributed to the large variation in casualty rates associated with different damage states of a given building type (see Tables 12-3 to 12-11 of FEMA, 2018); this type of uncertainty can be mitigated by adopting more sophisticated casualty models that explicitly capture potential injuries and fatalities associated with building-specific structural and non-structural components (e.g., FEMA, 2018).

4.6 Decision Module

The initial risk metrics are discussed with hypothetical stakeholders in Futureville, whose feedback leads to several modifications. The stakeholders are interested in the expected proportion of total people displaced (PD_{total}) across all income bands and ages (Risk Metric #1), and would like to quantify the extent to which those in the low-income band disproportionally experience some losses related to residential damage. Due to the relatively low number of resulting casualties (predominantly minor injuries), which is insignificant compared to the potentially vast amount of people affected by cascading impacts of displacement and low-income residential damage (e.g., Watson et al., 2007; Chang-Richards et al., 2019; Mallick & Vogt, 2014; Office of the US Surgeon General, 2009), the stakeholders have chosen to neglect the third initial risk metric in the analysis (and it is therefore removed from consideration in subsequent calculations).

We leverage a modified version of the Poverty Exposure Bias Indicator introduced in Winsemius et al. (2018) - called the Poverty Bias Indicator (PBI ; Risk Metric #2) - to express the disproportional losses experienced by low-income households, as follows:

$$PBI = \frac{loss_{low}}{loss_{all}} - 1 \tag{7}$$

where $loss_{low}$ indicates the expected proportion of low-income households that experience loss due to self-funded residential repairs and $loss_{all}$ is the equivalent expected proportion of all households. A negative value of PBI indicates a pro-poor approach (i.e, the proportion of low-income households experiencing losses is less than average). The underlying data for Risk Metrics #1 and #2 may be derived from the results shown in Figures 6 and 7, so no additional iteration through the Engineering Impact Module and the Social Impact Module is necessary in this case.

A summary of Risk Metric #1 and #2 values are shown in Figure 8, for the three examined policies. Results for the case in which no policy is implemented are also shown for completeness. Among the Policies #1 to 3, it can be seen that Policy #1 is associated with the lowest (i.e., most pro-poor) value of PBI, but results in the largest expected proportion of people displaced. Policy #3 produces the highest (and therefore worst) value of PBI, but is expected to result in a lower level of population displacement than both

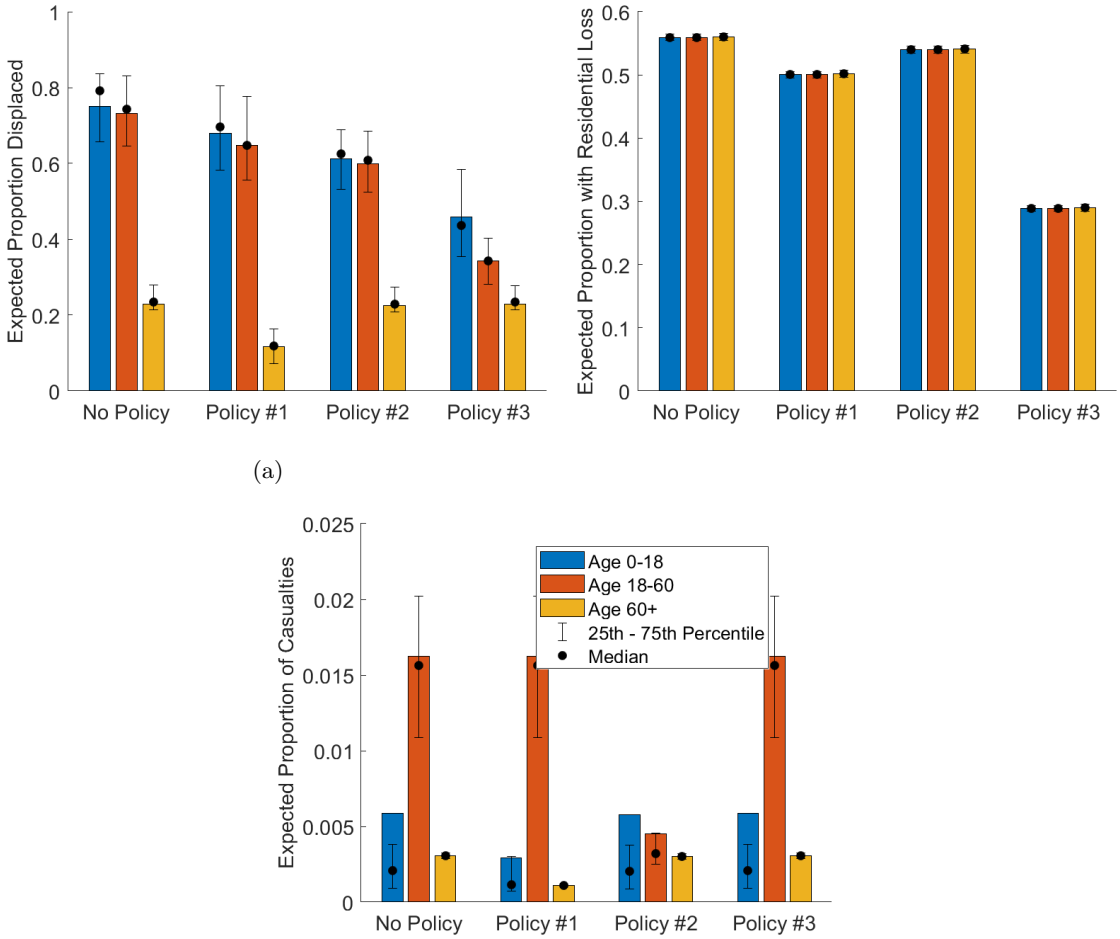

Figure 6: (a) Proportion of the population that will be dislocated, (b) Proportion of the population that will need to self-fund some repair costs for residential damage, and (c) Proportion of casualties, across the three examined policies and if no policy is implemented, disaggregated by age.

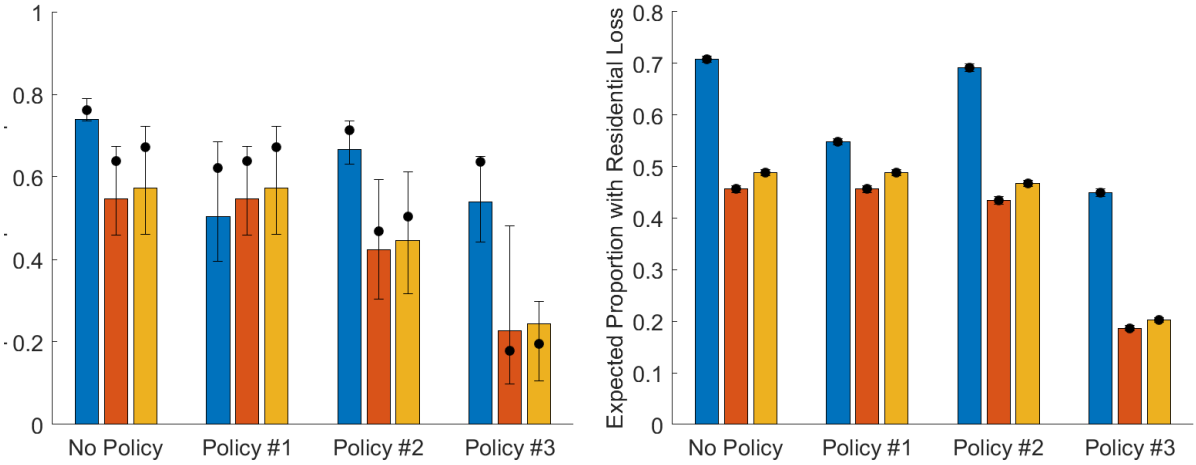

(a)

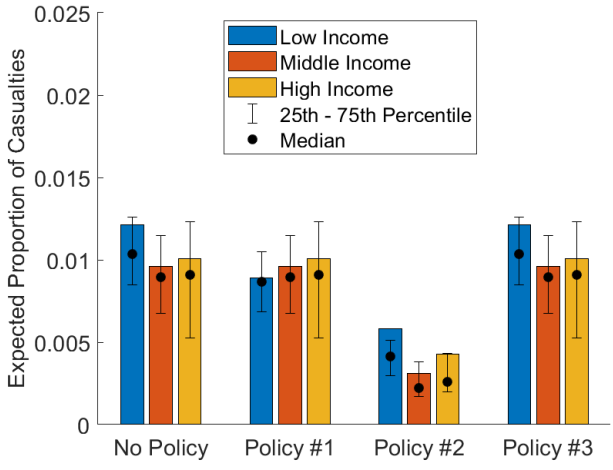

Figure 7: (a) Proportion of the population that will be dislocated, (b) Proportion of the population that will need to self-fund some repair costs for residential damage, and (c) Proportion of casualties, across the three examined policies and if no policy is implemented, disaggregated by income bracket.

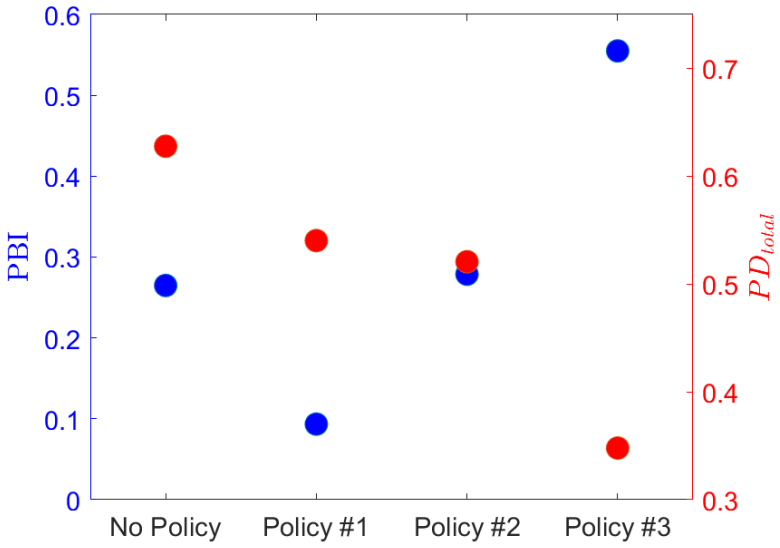

Figure 8: Values of PBI and PD_{total} risk metrics across the three examined policies and if no policy is implemented.

other policies. Policy #2 produces intermediate results for both metrics. The "No Policy" case leads to a worse outcome than any examined policy in terms of population displacement. However, it is associated with a much smaller PBI value than Policy #3, indicating that doing nothing is a more pro-poor strategy than offering post-disaster repair assistance for minor damage (at least for the scenario earthquake examined, which results in the strongest shaking in the low-income Zone 3 - see Figure 2(b).

We assume that the finalised risk metrics are weighted according to the analytic hierarchy process (see Section 3). Stakeholder feedback has suggested that it is equally important to minimise both metrics, so $w_1 = w_2 = 0.5$.

4.7 Policy with Lowest Overall Risk

We leverage the TOPSIS multi-criteria decision-making methodology (see Section 3) to compare the risk associated with the $n_{policy} = 3$ examined policies. A summary of S_i values for each examined policy is provided in Table 3. It can be seen that Policy #1 is the best option in this case.

Table 3: S_i values for the three examined policies. Bold font indicates the optimum policy selection.

Weighting Scheme	S_1	S_2	S_3
$w_1 = w_2 = 0.5$	**0.76**	0.55	0.24

5 Sensitivity Analyses

The case study of the proposed framework presented in Section 4 relied on a number of assumptions and hypothetically known details related to the data required for all modules. The purpose of this section is to demonstrate the versatility of the framework, by investigating the impact on the overall results of some alternative assumptions and additional uncertainties in the underlying data.

The first sensitivity analysis (herein referred to as "SA #1") alters the Seismic Hazard Module, by replacing the scenario earthquake with a fully deterministic magnitude 6 rupture that is located 20 km closer to Futureville. (Note that the GMM and spatial correlation model remain unchanged, and the set of ground-motion fields that forms the basis of the scenario is chosen using the procedure outlined in Section 4.1).

The second sensitivity analysis (consequently labelled as "SA #2") modifies the Engineering Impact Module, by assuming that the seismic resistance of current buildings degrades with age. The dynamic vulnerability of engineered assets is an important consideration for seismic risk analyses (Lallemant et al., 2017) that is often overlooked in conventional risk assessments (Lallemant, 2015). For this analysis, the median values of the fragility functions associated with each current building are independently reduced by a uniformly distributed factor between 0.2 and 0.3 in each Monte Carlo iteration of the computation, which is broadly in line with the 25-year aging effects on vulnerability found in Karapetrou et al. (2017). (Note that all retrofits included in Policies #1 and #2 are assumed to take place today, and are therefore also affected by reduced vulnerability in SA #2).

The third sensitivity analysis (henceforth regarded as "SA #3") investigates the implications of not knowing the breakdown of employment industry by income grouping. In this case, the work zone of each household for a given Monte Carlo simulation is randomly sampled (with equal likelihood) from retail/business, light industry, and heavy industry. (Retail/business workers within Zones 1 to 3 and Zones 6 to 9 are still assumed to work in Zones 4 and 9, respectively).

The PBI and PD_{total} risk metric values associated with each analysis are summarised in Figure 9. The general trend in risk-metric values is the same across each SA; Policy #1 always leads to the lowest value of PBI, whereas PD_{total} is consistently minimised by applying Policy #3. However, there is noteworthy variation in the absolute values of the risk metrics for different analyses. In particular, it is interesting to note that SA #1 results in lower PBI values, implying that the location of the selected scenario earthquake requires careful consideration when evaluating the pro-poor effect of a given policy. Values of PD_{total} are significantly higher than those of the original Section 4 calculations and less conservative PBI values are obtained if the vulnerability of existing structures degrades in time, further underlining the importance of considering this possibility when evaluating future risks. Another interesting observation is that SA #3 produces near-equivalent PD_{total} results to those of the original calculations (note that SA #3 does not influence PBI values, which exclusively relate to residential damage). However, it is important to note that SA #3 does lead to notable changes in the expected proportion of people displaced within given income brackets, and therefore the appropriate inclusion of uncertainties in the Social Impact Module can be crucial for accurately characterising certain risk metrics.

The final part of this section evaluates the optimum policy for each SA and various alternative potential stakeholder risk priorities (i.e., different values of w_j in equations 3 and 4) that may arise due to diverse political outlooks, for instance: $w_1 = 0.5, w_2 = 0.5$ (reducing PBI and reducing PD_{total} are equally important), $w_1 = 0.9, w_2 = 0.1$ (reducing population displacement is prioritised), and $w_1 = 0.1, w_2 = 0.9$ (reducing poverty bias in losses is prioritised). Table 4 presents the resulting S_i values for each SA,

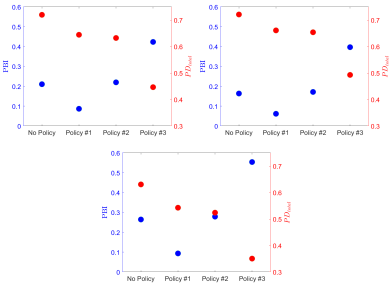

(a)

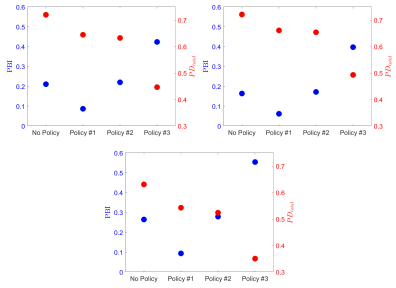

(b)

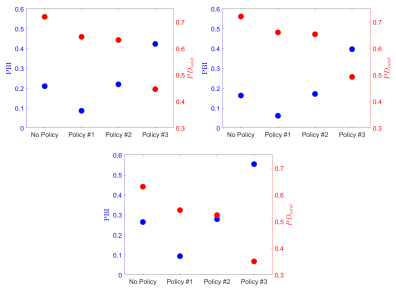

(c)

Figure 9: Values of PBI and PD_{total} risk metrics across the three examined policies and if no policy is implemented, for (a) SA #1, (b) SA #2, and (c) SA #3.

Table 4: S_i values for the three examined policies across SA #1, SA #2, and SA #3. S_i values associated with the original calculations in Section 4 are also shown for completeness. Bold font indicates the optimum policy selection.

Weighting Scheme	S_1	S_2	S_3
Original Calculations (Section 4)			
$w_1 = w_2 = 0.5$	**0.76**	0.55	0.24
$w_1 = 0.9, w_2 = 0.1$	0.26	0.20	**0.74**
$w_1 = 0.1, w_2 = 0.9$	**0.97**	0.60	0.03
SA #1			
$w_1 = w_2 = 0.5$	**0.78**	0.56	0.22
$w_1 = 0.9, w_2 = 0.1$	0.28	0.20	**0.72**
$w_1 = 0.1, w_2 = 0.9$	**0.97**	0.60	0.03
SA #2			
$w_1 = w_2 = 0.5$	**0.83**	0.64	0.17
$w_1 = 0.9, w_2 = 0.1$	0.35	0.27	**0.65**
$w_1 = 0.1, w_2 = 0.9$	**0.98**	0.67	0.02
SA #3			
$w_1 = w_2 = 0.5$	**0.76**	0.55	0.24
$w_1 = 0.9, w_2 = 0.1$	0.26	0.20	**0.74**
$w_1 = 0.1, w_2 = 0.9$	**0.97**	0.60	0.03

as well as for the original calculations. All of the various analyses lead to the same conclusion. Policy #1 is the best option if equal importance is placed on both risk types and if adopting a pro-poor approach is prioritised, whereas Policy #3 is the optimum selection if stakeholders place higher importance on minimising population displacement. The equivalent ultimate findings of each analysis is not unexpected, given the same general trend in risk-metric values that was observed for each policy in Figures 8 and 9.

6 Conclusions

This paper has introduced an end-to-end simulation-based framework for modelling risks associated with future earthquakes, which addresses some significant gaps associated with state-of-practice approaches to future seismic risk assessment. The framework may be leveraged to support decision making on urban planning/design and/or related policies, accounting for varied stakeholders perspectives and priorities around the concept of risk.

We demonstrated the framework using the hypothetical city of "Futureville", which was conceived on the basis of completely synthetic physical and socio-demographic data. In particular, we showcased the framework's ability to determine the optimum among a set of potential earthquake risk-reduction policies, considering the risk dimensions of interest to stakeholders and a multitude of uncertainties inherent in future projections of urban landscapes. We ultimately determined that the optimum policy can change depending on stakeholder's priorities towards different risk types. This finding, which mirrors the conclusions of similar studies in different contexts (e.g., Cremen & Galasso, 2021), underlines the critical importance of a collaborative risk assessment process that integrates stakeholder participation, capacity and feedback (Galasso et al., 2021). For the specific case study examined, it was found that a "soft policy" of providing post-disaster financial assistance for city inhabitants is the best option if stakeholders are most inter-

ested in minimising population displacement, whereas a "hard policy" of replacing low-income housing and facilities with code-compliant buildings is the optimal solution for stakeholders who are particularly motivated to reduce the relative burden of financial loss on the city's poorest.

While the hypothetical case study used was relatively limited in scope (i.e., considered only two or three risk metrics, incorporated a simplified earthquake scenario calculated purely on the basis of statistical models, and made a number of elementary assumptions on the city's functionality), we further demonstrated that the proposed framework is versatile enough for accommodating flexible (and potentially more realistic) data in each of its core modules, through a series of sensitivity analyses that altered the hypothetical inputs and/or amplified the uncertainties present in the underlying calculations. The ultimate conclusions of the study remained unchanged in these supplementary analyses. However, variations in the absolute values of the risk metrics obtained underline the importance of accurately characterising the input data and the associated uncertainties, which the proposed framework is explicitly designed to facilitate. We anticipate that the framework has the potential to play a leading role in preparing societies for future challenges related to earthquake hazards, directly addressing a need outlined in both the Sendai Framework for Disaster Risk Reduction (Aitsi-Selmi et al., 2016) and the United Nations Sustainable Development Goal 11 (Sustainable Cities and Communities; Assembly, 2015).

Finally, while this specific paper focuses on earthquake ground-shaking risk, the proposed framework can be easily extended to more earthquake-related hazards (e.g., liquefaction, tsunami inundation) or other (multiple) natural hazards with some ad-hoc modifications. For instance, tsunami inundation would require relevant tsunami intensity measures (e.g., peak velocity, momentum flux) to be output from the "Seismic Hazard Module". Future risks from river and flash flood hazard in urban/rural environments could be modelled by switching the positions of the Hazard and Engineering Impact Modules. This alteration would be necessary to account for the hazard's dependence on environmental change resulting from socioeconomic development; the expansion of impermeable surfaces (e.g., concrete or paved surfaces replacing natural ground cover) decreases infiltration and increases runoff during precipitation events.

Acknowledgments

We acknowledge funding from UKRI GCRF under grant NE/S009000/1, Tomorrow's Cities Hub. We thank Connie Hale, Center for Risk-Based Community Resilience Planning at Colorado State University, for providing the shapefiles of the Centerville Virtual Community. Data created will be made available on Github at `https://github.com/gcrem/`, upon acceptance of the manuscript.

References

Adnan, M. S. G., Abdullah, A. Y. M., Dewan, A., & Hall, J. W. (2020). The effects of changing land use and flood hazard on poverty in coastal bangladesh. *Land Use Policy*, *99*, 104868.

Aitsi-Selmi, A., Murray, V., Wannous, C., Dickinson, C., Johnston, D., Kawasaki, A., ... Yeung, T. (2016). Reflections on a science and technology agenda for 21st century disaster risk reduction. *International Journal of Disaster Risk Science*, *7*(1), 1–29.

Assembly, G. (2015). Sustainable development goals. *SDGs Transform Our World*, *2030*.

Baker, J. W. (2015). Efficient analytical fragility function fitting using dynamic structural analysis. *Earthquake Spectra*, *31*(1), 579–599.

Bonstrom, H., Corotis, R., & Porter, K. (2012). Overcoming public and political

challenges for natural hazard risk investment decisions. *Journal of Integrated Disaster Risk Management*, *2*(1).

Boore, D. M., Stewart, J. P., Seyhan, E., & Atkinson, G. M. (2014). Nga-west2 equations for predicting pga, pgv, and 5% damped psa for shallow crustal earthquakes. *Earthquake Spectra*, *30*(3), 1057–1085.

Bradley, B. A. (2019). On-going challenges in physics-based ground motion prediction and insights from the 2010–2011 canterbury and 2016 kaikoura, new zealand earthquakes. *Soil Dynamics and Earthquake Engineering*, *124*, 354–364.

Calderón, A., & Silva, V. (2021). Exposure forecasting for seismic risk estimation: Application to costa rica. *Earthquake Spectra*, 8755293021989333.

Chang-Richards, A., Seville, E., Wilkinson, S., & Walker, B. (2019). Effects of disasters on displaced workers. In *Resettlement challenges for displaced populations and refugees* (pp. 185–195). Springer.

Cremen, G., & Galasso, C. (2021). A decision-making methodology for risk-informed earthquake early warning. *Computer-Aided Civil and Infrastructure Engineering*.

Cremen, G., Seville, E., & Baker, J. W. (2020). Modeling post-earthquake business recovery time: An analytical framework. *International Journal of Disaster Risk Reduction*, *42*, 101328.

Cremen, G., Werner, M. J., & Baptie, B. (2020). A new procedure for evaluating ground-motion models, with application to hydraulic-fracture-induced seismicity in the united kingdom. *Bulletin of the Seismological Society of America*, *110*(5), 2380–2397.

Daniell, J., Simpson, A., Murnane, R., Tijssen, A., Nunez, A., Deparday, V., ... Schäfer, A. (2014). Review of open source and open access software packages available to quantify risk from natural hazards. *Washington, DC: World Bank and Global Facility for Disaster Reduction and Recovery*.

Ellingwood, B. R., Cutler, H., Gardoni, P., Peacock, W. G., van de Lindt, J. W., & Wang, N. (2016). The centerville virtual community: A fully integrated decision model of interacting physical and social infrastructure systems. *Sustainable and Resilient Infrastructure*, *1*(3-4), 95–107.

Elnashai, A., Hampton, S., Lee, J. S., McLaren, T., Myers, J. D., Navarro, C., ... Tolbert, N. (2008). Architectural overview of maeviz–hazturk. *Journal of Earthquake Engineering*, *12*(S2), 92–99.

Esposito, S., Iervolino, I., d'Onofrio, A., Santo, A., Cavalieri, F., & Franchin, P. (2015). Simulation-based seismic risk assessment of gas distribution networks. *Computer-Aided Civil and Infrastructure Engineering*, *30*(7), 508–523.

FEMA. (2018). *FEMA P-58-1: Seismic Performance Assessment of Buildings. Volume 1–Methodology*. Federal Emergency Management Agency Washington, DC.

FEMA. (2018). *HAZUS 4.2: Earthquake model technical manual*. Federal Emergency Management Agency (FEMA) Washington, DC.

Freddi, F., Galasso, C., Cremen, G., DallAsta, A., Di Sarno, L., Giaralis, A., ... others (2021). Innovations in earthquake risk reduction for resilience: Recent advances and challenges. *International Journal of Disaster Risk Reduction*, 102267.

Galasso, C., McCloskey, J., Pelling, M., Hope, M., Bean, C., Cremen, G., ... others (2021). Risk-based, pro-poor urban design and planning for tomorrows cities. *International Journal of Disaster Risk Reduction*.

Gautam, D., Fabbrocino, G., & de Magistris, F. S. (2018). Derive empirical fragility functions for nepali residential buildings. *Engineering Structures*, *171*, 617–628.

Graves, R., Jordan, T. H., Callaghan, S., Deelman, E., Field, E., Juve, G., ... others (2011). Cybershake: A physics-based seismic hazard model for southern

california. *Pure and Applied Geophysics*, *168*(3), 367–381.

Guidotti, R., Chmielewski, H., Unnikrishnan, V., Gardoni, P., McAllister, T., & van de Lindt, J. (2016). Modeling the resilience of critical infrastructure: The role of network dependencies. *Sustainable and resilient infrastructure*, *1*(3-4), 153–168.

Habitat, U. (2020). *World cities report 2020: The value of sustainable urbanization.* United Nations.

Iacoletti, S., Cremen, G., & Galasso, C. (2021). Advancements in multi-rupture time-dependent seismic hazard modeling, including fault interaction. *Earth-Science Reviews*, 103650.

Jayaram, N., & Baker, J. W. (2009). Correlation model for spatially distributed ground-motion intensities. *Earthquake Engineering & Structural Dynamics*, *38*(15), 1687–1708.

Karapetrou, S., Fotopoulou, S., & Pitilakis, K. (2017). Seismic vulnerability of rc buildings under the effect of aging. *Procedia environmental sciences*, *38*, 461–468.

Lallemant, D. (2015). *Modeling the future disaster risk of cities to envision paths towards their future resilience* (Unpublished doctoral dissertation). Stanford University.

Lallemant, D., Burton, H., Ceferino, L., Bullock, Z., & Kiremidjian, A. (2017). A framework and case study for earthquake vulnerability assessment of incrementally expanding buildings. *Earthquake spectra*, *33*(4), 1369–1384.

Mallick, B., & Vogt, J. (2014). Population displacement after cyclone and its consequences: Empirical evidence from coastal bangladesh. *Natural hazards*, *73*(2), 191–212.

Maqsood, T., Edwards, M., Ioannou, I., Kosmidis, I., Rossetto, T., & Corby, N. (2016). Seismic vulnerability functions for australian buildings by using gem empirical vulnerability assessment guidelines. *Natural Hazards*, *80*(3), 1625–1650.

Markhvida, M., Walsh, B., Hallegatte, S., & Baker, J. (2020). Quantification of disaster impacts through household well-being losses. *Nature Sustainability*, 1–10.

Martins, L., & Silva, V. (2020). Development of a fragility and vulnerability model for global seismic risk analyses. *Bulletin of Earthquake Engineering*, 1–27.

Miller, M., & Baker, J. W. (2016). Coupling mode-destination accessibility with seismic risk assessment to identify at-risk communities. *Reliability Engineering & System Safety*, *147*, 60–71.

Molina, S., Lang, D. H., & Lindholm, C. D. (2010). Selena–an open-source tool for seismic risk and loss assessment using a logic tree computation procedure. *Computers & Geosciences*, *36*(3), 257–269.

Mondoro, A., Frangopol, D. M., & Liu, L. (2018). Bridge adaptation and management under climate change uncertainties: A review. *Natural Hazards Review*, *19*(1), 04017023.

Motamed, H., Ghafory-Ashtiany, M., Amini-Hosseini, K., Mansouri, B., & Khazai, B. (2020). Earthquake risk–sensitive model for urban land use planning. *Natural Hazards*, *103*, 87–102.

Muis, S., Güneralp, B., Jongman, B., Aerts, J. C., & Ward, P. J. (2015). Flood risk and adaptation strategies under climate change and urban expansion: A probabilistic analysis using global data. *Science of the Total Environment*, *538*, 445–457.

Office of the US Surgeon General. (2009). The surgeon general's call to action to promote healthy homes.

Pitilakis, K., Karapetrou, S., & Fotopoulou, S. (2014). Consideration of aging and ssi effects on seismic vulnerability assessment of rc buildings. *Bulletin of Earthquake Engineering*, *12*(4), 1755–1776.

Porter, K., Kennedy, R., & Bachman, R. (2007). Creating fragility functions for performance-based earthquake engineering. *Earthquake Spectra*, *23*(2), 471–489.

Saaty, T. L. (1980). *The analytic hierarchy process: planning, priority setting, resource allocation*. New York: McGraw-Hill International Book Co,.

Scolobig, A., Prior, T., Schröter, D., Jörin, J., & Patt, A. (2015). Towards people-centred approaches for effective disaster risk management: Balancing rhetoric with reality. *International Journal of Disaster Risk Reduction*, *12*, 202–212.

Seto, K. C., Güneralp, B., & Hutyra, L. R. (2012). Global forecasts of urban expansion to 2030 and direct impacts on biodiversity and carbon pools. *Proceedings of the National Academy of Sciences*, *109*(40), 16083–16088.

Silva, V., Akkar, S., Baker, J., Bazzurro, P., Castro, J. M., Crowley, H., ... others (2019). Current challenges and future trends in analytical fragility and vulnerability modeling. *Earthquake Spectra*, *35*(4), 1927–1952.

Silva, V., Crowley, H., Pagani, M., Monelli, D., & Pinho, R. (2014). Development of the openquake engine, the global earthquake models open-source software for seismic risk assessment. *Natural Hazards*, *72*(3), 1409–1427.

Stafford, P. J., Strasser, F. O., & Bommer, J. J. (2008). An evaluation of the applicability of the nga models to ground-motion prediction in the euro-mediterranean region. *Bulletin of earthquake Engineering*, *6*(2), 149–177.

Stewart, I. S., Ickert, J., & Lacassin, R. (2017). Communicating seismic risk: the geoethical challenges of a people-centred, participatory approach. *Annals of Geophysics*, *60*.

Stewart, M. G., & Deng, X. (2015). Climate impact risks and climate adaptation engineering for built infrastructure. *ASCE-ASME Journal of Risk and Uncertainty in Engineering Systems, Part A: Civil Engineering*, *1*(1), 04014001.

Sutley, E. J., van de Lindt, J. W., & Peek, L. (2017). Community-level framework for seismic resilience. i: Coupling socioeconomic characteristics and engineering building systems. *Natural Hazards Review*, *18*(3), 04016014.

United Nations. (2019). World population prospects: the 2019 revision. *Population division of the department of economic and social affairs of the United Nations Secretariat, New York*.

Verschuur, J., Koks, E., Haque, A., & Hall, J. (2020). Prioritising resilience policies to reduce welfare losses from natural disasters: A case study for coastal bangladesh. *Global Environmental Change*, *65*, 102179.

Walsh, B., & Hallegatte, S. (2020). Measuring natural risks in the philippines: Socioeconomic resilience and wellbeing losses. *Economics of Disasters and Climate Change*, 1–45.

Watson, J. T., Gayer, M., & Connolly, M. A. (2007). Epidemics after natural disasters. *Emerging infectious diseases*, *13*(1), 1.

Weatherill, G., Silva, V., Crowley, H., & Bazzurro, P. (2015). Exploring the impact of spatial correlations and uncertainties for portfolio analysis in probabilistic seismic loss estimation. *Bulletin of Earthquake Engineering*, *13*(4), 957–981.

Winsemius, H. C., Jongman, B., Veldkamp, T. I., Hallegatte, S., Bangalore, M., & Ward, P. J. (2018). Disaster risk, climate change, and poverty: assessing the global exposure of poor people to floods and droughts. *Environment and Development Economics*, *3*, 328–348.

Wyss, M. (2005). Human losses expected in himalayan earthquakes. *Natural Hazards*, *34*(3), 305–314.

Yang, D. Y., & Frangopol, D. M. (2019). Societal risk assessment of transportation networks under uncertainties due to climate change and population growth. *Structural Safety*, *78*, 33–47.

Yang, D. Y., & Frangopol, D. M. (2020). Risk-based portfolio management of civil infrastructure assets under deep uncertainties associated with climate change: a robust optimisation approach. *Structure and Infrastructure Engineering*,

16(4), 531–546.
Yoon, K. P., & Hwang, C.-L. (1995). *Multiple attribute decision making: an introduction*. Sage Publications.